ROYAL SOCIETY OF CHEMISTRY

PAPER

Check for updates

An S-shaped double helicene showing both multi-resonance thermally activated delayed fluorescence and circularly polarized luminescence†

John Marques dos Santos, [ID][a] Dianming Sun, [ID][a] Juan Manuel Moreno-Naranjo,[b] David Hall,[ac] Francesco Zinna, [ID][d] Seán T. J. Ryan,[b] Wenda Shi,[b] Tomas Matulaitis, [ID][a] David B. Cordes, [ID][a] Alexandra M. Z. Slawin, [ID][a] David Beljonne, [ID][c] Stuart L. Warriner, [ID][e] Yoann Olivier, [ID]*[f] Matthew J. Fuchter [ID]*[b] and Eli Zysman-Colman [ID]*[a]

We present the first example of a multi-resonant thermally activated delayed fluorescent (MR-TADF) extended helicene, **Hel-DiDiKTa**. This S-shaped double helicene exhibits sky-blue emission, a singlet–triplet energy gap, ΔE_{ST}, of 0.15 eV and narrow emission at a peak maximum of 473 nm with a full-width at half-maximum of 44 nm in toluene. The MR-TADF character is confirmed by the small degree of positive solvatochromism and temperature-dependent increase in intensity of the delayed emission. The chiroptical properties of the separated enantiomers are similar to other large helicenes with comparable dissymmetry values, but with the added benefit of MR-TADF. **(P)-Hel-DiDiKTa** is stable towards enantiomerization, with a Gibbs free energy of activation for enantiomerization ($\Delta G_e^{\ddagger}$) of 31 ± 2 kcal mol^{-1} at 298 K, a value similar to other reported double helicenes. **(P)-Hel-DiDiKTa** is also thermally stable, with a 5% weight loss at 399 °C revealed by thermogravimetric analysis (TGA). Thus, this study further strengthens the burgeoning area of chiral TADF emitters for use in cutting-edge optoelectronic and photocatalytic molecules and materials.

[a] *Organic Semiconductor Centre, EaStCHEM School of Chemistry, University of St Andrews, St Andrews, KY16 9ST, UK. E-mail: eli.zysman-colman@st-andrews.ac.uk*

[b] *Department of Chemistry, Molecular Sciences Research Hub, Imperial College London, White City Campus, London, W12 0BZ, UK.*
E-mail: m.fuchter@imperial.ac.uk

[c] *Laboratory for Chemistry of Novel Materials, University of Mons, 7000 Mons, Belgium*

[d] *Dipartimento di Chimica e Chimica Industriale, Università di Pisa, 56124 Pisa, Italy*

[e] *School of Chemistry, University of Leeds, Leeds, LS2 9JT, UK*

[f] *Laboratory for Computational Modeling of Functional Materials, Namur Institute of Structured Matter, Université de Namur, Rue de Bruxelles, 61, 5000 Namur, Belgium. E-mail: yoann.olivier@unamur.be*

† Electronic supplementary information (ESI) available: A summary of prior examples of carbonyl-containing MR-TADF emitters, experimental details, synthesis procedures and characterization data, NMR spectra, HRMS, HPLC, X-ray crystallographic data, supplemental photophysical data, electrochemical data, chiral HPLC, CD spectra, CPPL data, computational simulations, enantiomerisation kinetics data and thermogravimetric analysis. CCDC 2105660. For ESI and crystallographic data in CIF or other electronic format see DOI: 10.1039/d2tc00198e. The research data supporting this publication can be accessed at https://doi.org/10.17630/25585cf8-5f19-4b26-b95e-569787e10399.

Introduction

Helicenes are a class of fused polycyclic aromatic frameworks that possess a helically chiral framework,[1,2] where overlapping rings render the enantiomers kinetically stable to racemization. Helicenes usually display strong circular dichroism (CD)[3] and circularly polarized luminescence (CPL),[4–8] which has led them to be investigated in a number of different applications.[4,9] These include nonlinear optics,[10] chemical sensors,[11] asymmetric catalysis,[12,13] circularly polarised luminescent materials[14–16] and as ligands in Ir, Zn and Pt complexes,[9] the latter of which have been employed in phosphorescent CP-OLEDs.[17,18] They have also been exploited as fluorescent emitters,[5,19] chiral additives for induced chiral fluorescence polymers[20–23] and as components within donor–acceptor (D–A) TADF emitters[24,25] in CP-OLEDs. Beyond chiroptical properties the high solubility of helicenes in organic solvents (compared to planar acenes), coupled with their excellent thermal stability has led to a wider array of optoelectronic applications, including as hole-transport materials in photovoltaic devices.[26–28]

Thermally activated delayed fluorescence (TADF) materials have become increasingly attractive as sensors,[29] in lasers,[30]

photodetectors,[31] photocatalysis[32] and bioimaging[33] as well as both emitters and hosts in organic light-emitting diodes (OLEDs)[34] due to their ability to harvest 100% of electrically generated excitons to generate light. This is accomplished by conversion of triplet excitons into singlets *via* reverse inter-system crossing (RISC)[34–38] enabled by their small S_1–T_1 energy gap, ΔE_{ST}.[39] The dominant molecular design relies on a strongly twisted donor–acceptor architecture that minimises the overlap between the highest occupied molecular orbital (HOMO) and the lowest unoccupied molecular orbital (LUMO), resulting in a small ΔE_{ST}. This strategy also results in compounds with relatively large conformational flexibility and/or intra-molecular/stretching vibrations, which in turn leads to broad emission characterized by a full width half maximum (FWHM) typically greater than 80 nm, resulting in poor color purity in resulting OLED devices.[40] Hatakeyama and co-workers have advanced an alternative molecular design strategy to produce TADF materials with narrowband emission (FWHM < 40 nm), based on polycyclic aromatic hydrocarbons doped with electron-accepting B, and electron-donating N and O atoms.[41,42] These so-called multi-resonant TADF (MR-TADF) emitters rely on p- and n-doping of polycyclic aromatic hydrocarbons to limit the overlap between the HOMO and the LUMO electron-density and thus produce a small ΔE_{ST}, while their rigid molecular structure results in negligible conformational reorganization in the excited state, and narrowband emission.[40,42,43] There are now examples of blue,[44–48] green[48–52] and red[43,53,54] MR-TADF materials used as emitters in high-efficiency OLEDs.[55–57]

The study and exploitation of CPL has accelerated over the past decade due to a recognition that employing CPL-active compounds can lead to an increased efficiency of OLEDs and other optoelectronic devices.[17,58–62] Other technologies being investigated for the exploitation of CPL include quantum computing,[63,64] 3D information displays,[23,65] spintronic devices,[66] transistors,[67] CPL lasers[68] and biological probes.[69,70] The CPL intensity of a chiral molecule can be quantified by the dissymmetry factor, g_{PL}, which is represented by eqn (1):.[7,71,72]

$$g_{PL} = \frac{I_L - I_R}{\frac{1}{2}(I_L - I_R)} = \frac{4|\mu||m|\cos\theta}{|\mu|^2 + |m|^2} \quad (1)$$

Here, I_L and I_R refer to the intensity of left- and right-handed circularly polarised luminescence, respectively; μ is the electric transition dipole moment, m is the magnetic transition dipole moment and θ is the angle between the transition dipole moments. This expression reveals that the maximum attainable g_{PL} (which is ±2) is obtained when the transition dipole moments, μ and m, have the same magnitude ($|\mu|/|m|$ = 1) and are parallel or antiparallel ($\cos\theta$ = ± 1) to each other. Unfortunately, chiral molecules that display high photoluminescence quantum yields (Φ_{PL}) typically show small g_{PL} and *vice versa*.[15,16] For instance, lanthanoid complexes typically show high g_{PL} (0.1–1)[73–75] but in order to reach high brightness values[76] they need suitable antenna ligands to overcome the Laporte-forbidden nature of their transitions. In contrast, organic molecules can attain high absorption and emission intensities but typically show relatively

low g_{PL} ($\leq 10^{-2}$) due to their significantly larger electric transition dipole moments compared to their magnetic transition dipole moments, coupled with their relatively smaller molecular size.[7,8,77,78]

Presently, there exists a small number of organic compounds displaying CP-TADF, with most of the reports emerging over the past few years. A number of these have been used in CP-TADF OLEDs,[18,60,62,79,80] showing maximum external quantum efficiencies (EQE$_{max}$) surpassing 30%[80] but with g_{EL} typically $\leq 10^{-3}$ (Fig. 1a). The overwhelming majority of compounds showing CP-TADF are based on a donor–acceptor design that incorporates a remote stereogenic unit (asymmetric centre or axis) to induce chirality,[18,60,61,81–83] and so do not show narrow emission spectra. Materials showing concomitantly narrow emission, TADF and CPL are of significant interest, and a class of compounds that can meet these requirements are chiral MR-TADF compounds. To date, there exists only a handful of reports of chiral MR-TADF compounds. Compounds **OBN-2CN-BN** and **OBN-4CN-BN**,[84] were based loosely on Hatakeyama's DABNA-1[41] design and contain a peripheral chiral (*R/S*)-octahydro-binaphthol group that is not directly implicated in the emissive short-range charge transfer excited state.[84] A similar strategy was used for **QAO-PhCz**,[85] by introducing a 9-phenyl-9*H*-carbazole appended group to the MR-framework to lock the helical structure and obtain chirality. There are only two reports where the MR-TADF core structure shows intrinsic chirality and both are boron/nitrogen-based helicenes: compounds **BN5**[86] and **OBN-Cz** (aka **1a**).[87]

The first CPL data reported for helicenoids belong to two bridged triphenylamine diketone derivatives, reported by Venkataraman *et al.*, (renamed here as **Hel-DiKTa-3** and **Hel-DiKTa-4**, Fig. 1b) with g_{PL}: $-1.1 \times 10^{-3}/9 \times 10^{-4}$ at 453 nm for (*M*)-**Hel-DiKTa-3** and (*P*)-**Hel-DiKTa-3** and $-7 \times 10^{-4}/8 \times 10^{-4}$ at 478 nm for (*M*)-**Hel-DiKTa-4** and (*P*)-**Hel-DiKTa-4**, respectively.[14] Given our previous work on diketone-based MR-TADF emitters (namely **DiKTa** and **DDiKTa**, structures shown in Fig. S1, ESI†),[44,49] we envisaged that developing a helical analogue of **DiKTa** would be an elegant strategy to obtain a CPL-active molecule without compromising MR-TADF. Our preliminary quantum calculations for **Hel-DiKTa-2**[88] (Fig. 1a, renamed here for clarity), however, revealed that its ΔE_{ST} is too large (0.51 eV) for it to show MR-TADF due to triplet stabilization on the naphthalene group (*vide infra*).

Here we report an intrinsically helically chiral MR-TADF molecule that is CPL-active and is based on an extended helicene structure, **Hel-DiDiKTa** (Fig. 1b); an S-shaped double [4]helicene. Despite a large current interest in multiple helicenes, the chiroptical properties of these molecules remain understudied.[89] We report in-depth structural, photophysical and chiroptical data for **Hel-DiDiKTa** and believe our study paves the way for further chiral MR-TADF molecules, based on extended or multiple helicene frameworks.

The synthesis of **Hel-DiDiKTa** is shown in Scheme 1a. A Cu-catalysed Ullman coupling between *m*-phenylenediamine and methyl 2-iodobenzoate afforded intermediate **1** in moderate yield (43%). Saponification proceeded quantitatively to yield **2**,
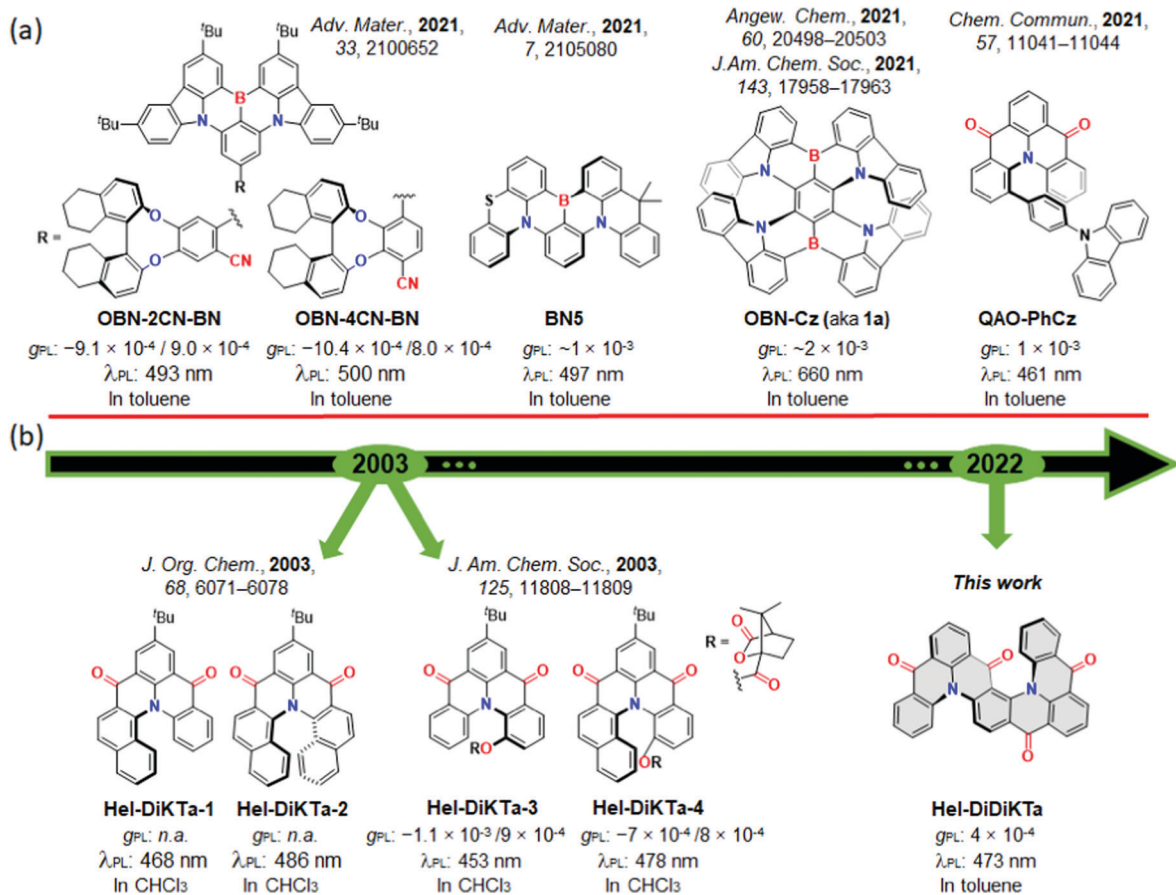
4862 | *J. Mater. Chem. C*, 2022, **10**, 4861–4870

This journal is © The Royal Society of Chemistry 2022

Fig. 1 (a) Structure of prior examples of MR-TADF materials able to display CPL.[84–87] (b) Structure of prior examples of triangulene helicenes and **Hel-DiDiKTa**.[14,88]

which was then subjected to a four-fold intramolecular Friedel–Crafts acylation of the *in situ*-prepared acyl chloride derivative in the presence of the Lewis acid $AlCl_3$ to afford the title compound, (*rac*)-**Hel-DiDiKTa**, in 36% yield as a racemate; the C-shaped compound **QA-2**, which was recently reported by Yasuda *et al.*[45] using a different synthetic route (and crystallised as a non-chiral
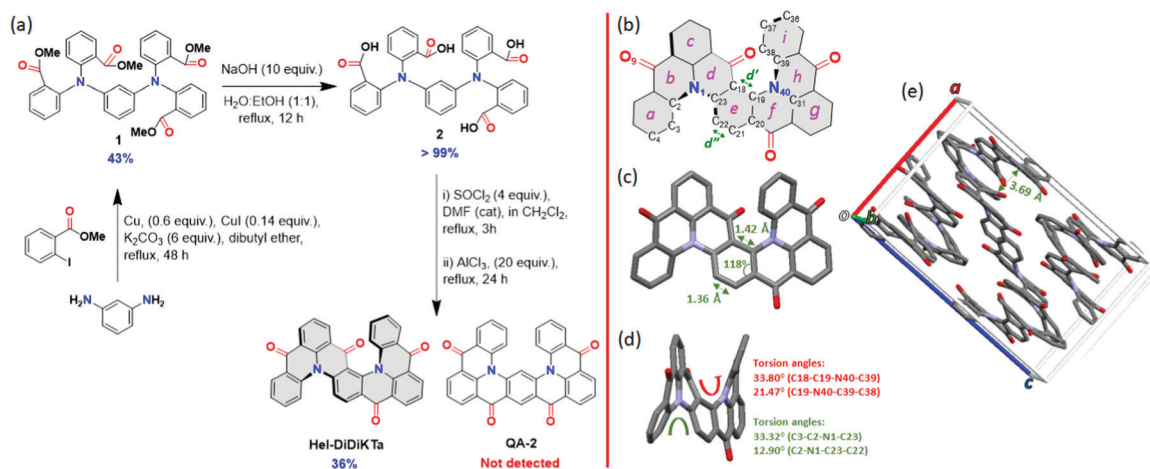
Scheme 1 (a) Synthesis of **Hel-DiDiKTa**. (b) Schematic of molecular structure of **Hel-DiDiKTa** showing atom labels (double bonds omitted for clarity). (c) View showing **Hel-DiDiKTa** in the crystal structure (front view) (internal bond angles: 119.42(10)° (C18-C19-C20), 118.73(10)° (C19-C20-C21), 122.54(10)° (C20-C21-C22), 119.41(10)° (C21-C22-C23), 119.12(9)° (C22-C23-C18) and 119.39(9)° (C23-C18-C19)) and (d) side view showing the helical pitch of **Hel-DiDiKTa** (torsion angles: 33.32° (C3-C2-N1-C23), 12.90° (C2-N1-C23-C22), 33.80° (C18-C19-N40-C39) and 21.47° (C19-N40-C39-C38)) (H atoms omitted for clarity). (e) Packing diagram of **Hel-DiDiKTa** viewed down the crystallographic *b*-axis.

This journal is © The Royal Society of Chemistry 2022

J. Mater. Chem. C, 2022, **10**, 4861–4870 | **4863**

meso isomer), was not detected. We performed Density Functional Theory (DFT) and coupled cluster calculations to probe which of the two products, (*rac*)-**Hel-DiDiKTa** or **QA-2**, is more stable in the ground state. **QA-2** was calculated to be more stable than **Hel-DiDiKTa** by between 18 and 29 kJ mol^{-1}, irrespective of the methodology applied (Fig. S19 and Table S7, ESI†), thus (*rac*)-**Hel-DiDiKTa** represents the kinetic product. The identity and purity of **Hel-DiDiKTa** was established by a combination of NMR spectroscopy, HRMS, melting point determination, HPLC measurements and elemental analysis. Additionally, single crystals of sufficient quality were grown by slow evaporation of a CH_2Cl_2 : EtOAc solution (7 : 3 ratio), enabling determination of the single crystal structure.

Crystallographic data of **Hel-DiDiKTa** obtained by single crystal X-ray diffraction revealed that the compound crystallizes as a racemate. The helical pitch through each of the two [4]helicenes varies between 12.90(15) and 33.80(15)° (torsion angles C3-C2-N1-C23, C2-N1-C23-C22, C18-C19-N40-C39 and C19-N40-C39-C38) and is similar to that found in **DiKTa** (27.2°) (Scheme 1d). Typically, in helicenes, the benzene ring at the centre of the helical structure is distorted, with two very different C–C bond lengths; a longer C–C bond facing the inner helix and opposite it a much shorter one facing the outer helix (distances *d'* and *d''* in Scheme 1b). This also leads to internal bond angles that are considerably different from that of an ideal planar benzene ring. This is not usually the case for S-shaped double helicenes,[90–93] and as such, in **Hel-DiKTa**, the

central benzene e-ring (Scheme 1b) has internal bond angles between 118.73(10) and 122.54(10)° and C–C bond distances between 1.3641(17) and 1.4207(15) Å (Scheme 1c). There is only one π−π stacking interaction between adjacent molecules (packing diagram displayed in Scheme 1e), the *c*-ring interacting with the *g*-ring [centroid···centroid distance 3.6875(6) Å], resulting in π-stacked chains running along the *b*-axis.

Cyclic voltammetry (CV) and differential pulse voltammetry (DPV) recorded in degassed dichloromethane (Fig. 2a) revealed an irreversible oxidation wave at E_{ox} = 1.81 V *vs.* SCE and a reversible reduction wave at E_{red} = −1.16 V *vs.* SCE. The corresponding HOMO and LUMO energy levels are −6.15 and −3.18 eV, respectively. The LUMO is only slightly stabilized compared to that of the parent compounds **DiKTa** (−3.11 eV) while the HOMO is considerably more stabilized than that of **DiKTa** (−5.93 eV).[44] The electrochemical data are summarized in Table S6 (ESI†).

The UV-vis absorption spectrum of (*rac*)-**Hel-DiDiKTa** in toluene (Fig. 2b and Fig. S8a, ESI†) is significantly different than that of **DiKTa**. There is a high-energy, high-intensity band at 360 nm (ε = 10 917 M^{-1} cm^{-1}) assigned by Spin-Component Scaling second-order approximate Coupled-Cluster (SCS-CC2) calculations as a π−π* transition centered on one half of the emitter (Fig. S23, ESI†). There is a higher-intensity, low-energy band at 425 nm (ε = 21 140 M^{-1} cm^{-1}) assigned as a short-range charge-transfer (SRCT) transition, which, according to the calculations, is associated with a transition to the S$_2$ state at
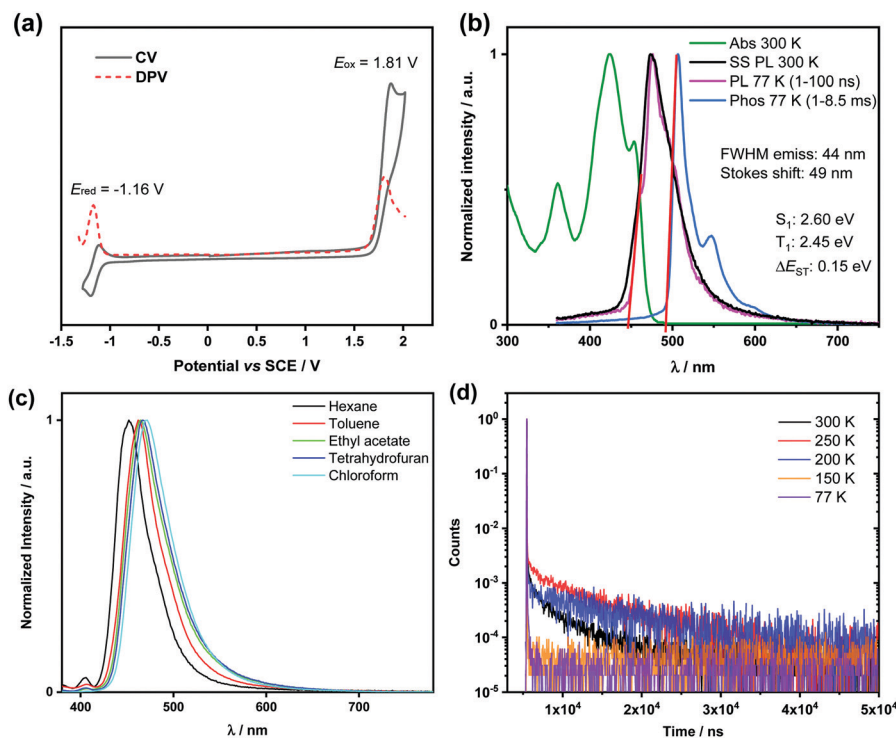

Fig. 2 Optoelectronic characterization of (*rac*)-**Hel-DiDiKTa**: (a) cyclic and differential pulse voltammograms in degassed CH_2Cl_2 with 0.1 m [^{n}Bu$_4$N]PF$_6$ as the supporting electrolyte and Fc/Fc$^+$ as the internal reference (Fc/Fc$^+$ = 0.46 V *vs.* SCE).[94] (b) Absorption (green line) and steady-state (SS) PL spectra obtained in toluene at 300 K (black line) and 77 K (pink line), and phosphorescence (Phos.) spectrum in toluene glass at 77 K (blue line) (delay: 1 ms; gate time: 8.5 ms, λ_{exc} = 343 nm). (c) Solvatochromic PL study (λ_{exc} = 350 nm). (d) Temperature-dependent lifetime for 1 wt% (*rac*)-**Hel-DiDiKTa** in mCP.

4864 | *J. Mater. Chem. C*, 2022, **10**, 4861–4870

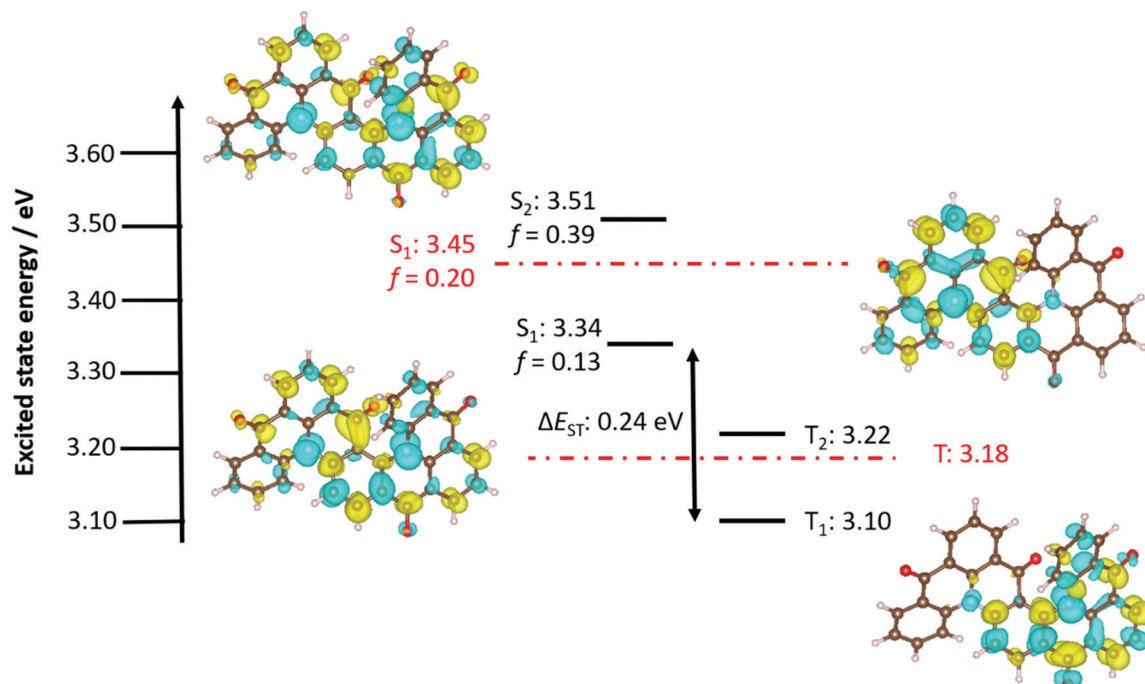This journal is © The Royal Society of Chemistry 2022

Fig. 3 Difference density plots computed at SCS-CC2/cc-pVDZ level considering only one-electronic transition contributions for (*rac*)-**Hel-DiDiKTa**. The red dashed lines show the energy levels for **DiKTa**.

3.51 eV. The band at 453 nm is associated with a transition to the S_1 state, and has a lower ε of 14 292 M^{-1} cm^{-1} than the band at 425 nm; a trend in line with the lower calculated oscillator strength, f, of 0.13 for S_1 compared to 0.39 for S_2. This assignment is further corroborated by the energy difference between these states, calculated to be 0.17 eV (Fig. 3) and measured to be 0.18 eV (Fig. 2b). S_1 is also SRCT in nature, with S_1 centered more around the middle of the molecule and S_2 associated with electronic density across the entire molecule, hence the oscillator strength changes (Fig. 3). This low-energy S_1 band is red-shifted compared to that of **DiKTa** (433 nm), with lower molar absorptivity (ε of **DiKTa** $\sim$21 000 M^{-1} cm^{-1})[44] in line with the change in energy of the S_1 state and the lower oscillator strength, which are 3.45 eV and 0.20 for **DiKTa**, and 3.34 eV and 0.13 for **Hel-DiDiKTa** (Fig. 3).

The room temperature steady-state (SS) photoluminescence (PL) spectrum of (*rac*)-**Hel-DiDiKTa**, recorded in toluene, peaks at 473 nm, which is slightly red-shifted compared to that of **DiKTa** (λ_{PL} = 453 nm). The PL spectrum is narrow (FWHM = 44 nm) and shows a small Stokes shift of 49 nm, both of which reflect the conformationally rigid structure and the small degree of geometrical relaxation in the excited state (Fig. 2b). This FWHM value is considerably smaller than many of the helicene compounds reported in the literature (often 50 – 80 nm).[1,16,19,81,91–93,95] The PL spectrum at 77 K is nearly identical to that at room temperature. Furthermore, a very small degree of positive solvatochromism is observed (Fig. 2c and Table S1, ESI†), behavior that is a hallmark of MR-TADF compounds.[44,96] Unlike *para*-disposed nitrogen and ketone groups that leads to a significant bathochromic shift in the emission compared to their *meta*-functionalized analogue, as evidenced in the case of the emitters **DMQA** and **QA-1** (c.f.,

Fig. S1, ESI†) recently reported by Yasuda *et al.*,[45] the emission energy of (*rac*)-**Hel-DiDiKTa** changes very little compared to that of **DiKTa**. This is despite of the increased conjugation length of **Hel-DiDiKTa** and is due to the *meta*-disposition of the amine and ketone groups. The S_1 and T_1, determined from the peaks of the prompt fluorescence and phosphorescence spectra in toluene at 77 K, respectively, are 2.60 and 2.45 eV, leading to a moderate ΔE_{ST} of 0.15 eV. These values are in reasonable accord with the predicted by SCS-CC2 calculations (ΔE_{ST} = 0.24 eV) and with those of other reported ketone-containing MR-TADF compounds, including **DiKTa** (0.20 eV).[44,45,49] The Φ_{PL} in toluene is very low at 1% and is due to significant non-radiative decay that is not uncommon in helicene compounds. No delayed emission was detected by time-resolved PL measurements in toluene (Fig. S13, ESI†). Recently, Wu *et al.* highlighted that many MR-TADF emitters, including N/ketone-based emitters, may not show TADF behavior in solvents while TADF can be observed in a suitable host due to exciplex-like host-emitter interactions.[97] The SS PL spectrum is only slightly affected by the presence of air (Fig. S9, ESI†). The Φ_{PL} improved to 4.1% as a 1 wt% doped film in 1,3-bis (N-carbazolyl)benzene (mCP) and to 6.2% in 1 wt% doped film in PMMA. We note that the Φ_{PL} remained essentially constant at $\sim$5% regardless of the doping concentration in mCP (Table S2, ESI†). These results are similar to the Φ_{PL} values reported for unsubstituted helicenes.[16]

In mCP (1 wt% of emitter) the SS spectrum peaks at 477 nm (Fig. S10a, ESI†), the FWHM value is 50 nm, and, in contrast to what is seen in toluene solution (Fig. S9, ESI†), both the PL intensity and lifetime of (*rac*)-**Hel-DiDiKTa** decrease moderately in the presence of O_2 (Fig. S10a and b, ESI†).

This journal is © The Royal Society of Chemistry 2022

J. Mater. Chem. C, 2022, **10**, 4861–4870 | **4865**

Temperature-dependent time-resolved PL measurements revealed an increase in the contribution of the delayed component of the emission decay with increasing temperature (Fig. 2d and Table S4, ESI†), which corroborates the TADF character of **Hel-DiDiKTa**. The S_1, T_1 and ΔE_{ST} values, determined from the peaks of the prompt fluorescence and phosphorescence spectra at 77 K, in mCP are 2.59, 2.44 and 0.15 eV, respectively, while in PMMA, these are essentially the same at 2.58, 2.45 and 0.13 eV, respectively. The temperature-dependent steady-state PL emission of (*rac*)-**Hel-DiDiKTa** was measured in 1% mCP, and the data are shown in Fig. S12 (ESI†). Analysis of the evolution of the SS PL of (*rac*)-**Hel-DiDiKTa** with decreasing temperature reveals a competition between phosphorescence and delayed fluorescence, with the phosphorescence intensity increasing considerably at lower temperatures (150 K and 77 K, Fig. S12, ESI†), which indicates that non-radiative decay is suppressed at lower temperatures and the phosphorescence becomes more competitive (Table S4, ESI†). We also observed from the temperature dependent transient decay profile of (*rac*)-**Hel-DiDiKTa** (1 wt% in mCP, Fig. 2d) that the delayed fluorescence intensity increases upon going from 300 K to 250 K, indicating decreased non-radiative decay due to suppression of molecular vibrations at 250 K. The delayed fluorescence intensity then decreases considerably upon reaching 77 K, which we ascribe to the quenching of the TADF (Table 1). The photophysical data is summarized in Table 1.

Density Functional Theory (DFT) calculations were first performed to optimize the geometry of the ground state, taking the crystal structure geometry as the starting point. Compared to **DiKTa** (−6.20 eV), the calculated HOMO energy is slightly stabilized to −6.26 eV for **Hel-DiDiKTa** (Table S8, ESI†). A larger stabilization of the LUMO energy exists at −2.53 eV (for **DiKTa**, E_{LUMO} = −2.23 eV). The relative HOMO/LUMO levels corroborate the experimental values of −5.93 eV/−3.11 eV for **DiKTa** and −6.15 eV/−3.18 eV for **Hel-DiDiKTa**. Previously, we have highlighted that DFT is not appropriate as it does not accurately predict the excited state energies of MR-TADF emitters.[96] We thus used Spin-Component Scaling second-order approximate Coupled-Cluster (SCS-CC2) calculations, which we have shown previously to provide an excellent set of predictions of ΔE_{ST} and S_1 energies.[44,49,98,99] SCS-CC2 calculations predict the S_1 state to be 3.34 eV and the T_1 state to be 3.10 eV, resulting in a ΔE_{ST} of 0.24 eV, which is slightly smaller than that calculated for **DiKTa** (ΔE_{ST} = 0.27 eV). The difference density plots are shown in Fig. 3

and reveal how the electronic density evolves from the ground state to the excited states. The pattern of the difference density plots for S_1 and S_2 is indicative of SRCT states involving the entirety of the helicene structure, while the plots for T_1 and T_2 likewise show the alternating increase and decrease in electron density pattern, but this is localized on different fragments of the helicene corresponding to the **DiKTa** core structure. The differences in orbital type between the singlet and triplet excited states ensure that RISC can occur directly between these states;[100] the presence of an intermediate triplet excited state should also facilitate RISC.[101–103] The SRCT character of the S_1 and T_1 states explains the moderate ΔE_{ST}. We also performed SCS-CC2 calculations on the previously reported compound **Hel-?A3B2 tlsb -0.045w?>DiKTa-2**. This compound possesses a very large ΔE_{ST} of 0.51 eV (Table S8, ESI†) due to triplet stabilisation by the naphthalene group[104] and so is unlikely to show TADF (Fig. S21, ESI†).

(*rac*)-**Hel-DiDiKTa** was separated into its *P*- and *M*-enantiomers using peak recycling chiral HPLC (*c*HPLC; Fig. S14, ESI†), demonstrating high enantiomeric excess (>99% and >97%, respectively; Fig. S15, ESI†). The circular dichroism (CD) spectra for the separated enantiomers were recorded in toluene (Fig. 4a) and showed mirror-image CD signals (Fig. S17, ESI† right), which exhibited multiple bisignate cotton effects throughout the ground state absorption spectral range (300–480 nm). Time-dependent DFT calculation (PBE0/6-31g(d,p)) was employed to predict the CD spectra and assign the absolute configuration (*P* and *M*) of **Hel-DiDiKTa** (Fig. S24, ESI†). The TD-DFT predicted CD spectra shown in Fig. S24 (ESI†) align with the CD spectra obtained experimentally. A maximum $|g_{abs}|$ of 2.8×10^{-3} was observed at 320 nm (Fig. S17, ESI†). These results are of a similar order of magnitude to other chiral small molecule TADF systems.[2,14] Circularly polarized photoluminescence (CPPL) spectra (Fig. S17, ESI†) display mirror image monosignate bands peaking at around 465 nm, confirming the transference of chirality to the excited state, with a maximum $|g_{PL}|$ of 4×10^{-4} for both enantiomers (Fig. S18, ESI†). These values are also similar to other helicenes and chiral small molecule TADF systems reported in the literature,[76] and align with those reported for helicenoids with two bridged triphenylamine diketone derivatives (10^{-4}–10^{-3}, see Fig. 1).[14] As expected for helicenes[7] where the ground and emitting excited state geometries are generally similar, the sign and magnitude of g_{PL} align with those of g_{abs} calculated at around 455 nm.

Table 1 Optoelectronic properties of (*rac*)-**Hel-DiDiKTa**

In toluene									In film					
$\lambda_{abs}{}^a$ /nm	ε^a/M^{-1} cm^{-1}	$\lambda_{PL}{}^b$ /nm	Φ_{PL} in N$_2$ (air)^c /%	FWHM^d/ nm (eV)	$S_1{}^e$/eV	$T_1{}^e$/eV	$\Delta E_{ST}{}^f$/eV		λ_{PL} /nm	Φ_{PL} in N$_2$ (air) /%	FWHM^d/ nm (eV)	S_1 /eV	T_1 /eV	ΔE_{ST} /eV
360/425/453	10 917/21 140/14 292	473	1.34 (1.27)	44 (0.25)	2.60	2.45	0.15		478^g	4.1 (4.0)^g	52 (0.29)^g	2.59^g	2.44^g	0.15^g
									480^h	6.2 (5.4)^h	58 (0.33)^h	2.58^h	2.45^h	0.13^h

^{a} UV-vis absorption band of interest. ^{b} PL in toluene degassing with N$_2$. ^{c} Photoluminescence quantum yield in toluene relative to quinine sulfate in 1 N H$_2$SO$_4$ (Φ_{PL} = 54.6%). ^{d} Full width at half maximum. ^{e} Obtained using an integrating sphere under N$_2$. ^{f} Energy gap between S_1 and T_1 calculated from the difference of the peaks of the fluorescence and phosphorescence spectra in toluene glass at 77 K. ^{g} 1 wt% (*rac*)-**Hel-DiDiKTa** doped in mCP. ^{h} 1 wt% (*rac*)-**Hel-DiDiKTa** doped in PMMA.
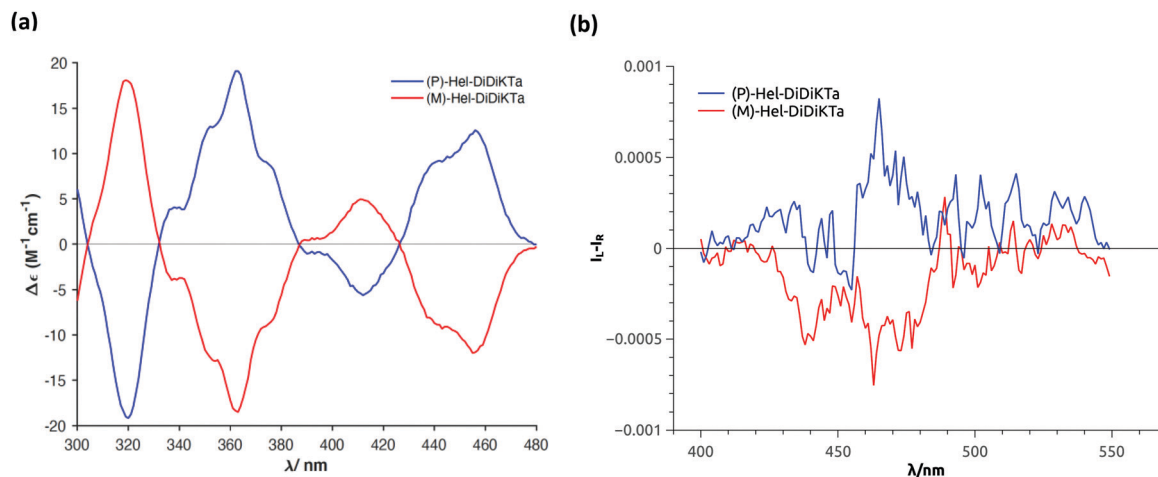
4866 | *J. Mater. Chem. C*, 2022, **10**, 4861–4870

This journal is © The Royal Society of Chemistry 2022

Fig. 4 (a) Circular dichroism and (b) CPL spectra for (**P**)-**Hel-DiDiKTa** (blue) and (**M**)-**Hel-DiDiKTa** (red) in toluene.

Upon optimization of the molecular structure at the lowest-energy singlet excited state (S_1) at the PBE0/6-31g(d,p) level of theory, we calculated a g_{PL} value of 6.94×10^{-4} (Table S9, ESI†), which aligns closely with the measured g_{PL}. The main limiting factor for the magnitude of g_{PL}, based on our calculations, is the nearly perpendicular alignment of the $|\mu|$ and $|m|$ vectors [$\cos\theta = 0.116918$ ($\theta = 83.28573$)]. Although the magnitude of $|m|$ is low at $0.348671679 \times 10^{-20}$ esu cm^{-1}, compared to $|\mu|$ ($234.811511 \times 10^{-20}$ erg G^{-1}), it is within the range typically observed for helicenes.[3,15,16,95] This result suggests that our molecular design is promising to generate strong CPL MR-TADF emitters if the alignment between $|\mu|$ and $|m|$ can be solved.[3,15,16,95] While these molecules do not have suitable Φ_{PL} to warrant exploration in OLEDs, they provide valuable insight into CP-TADF material design, particularly integrating MR-TADF into helicenes.

After the resolution of both enantiomers, the enantiomerisation process was studied. The CD signal decay from (**P**)-**Hel-DiDiKTa** in *p*-xylene at different temperatures (T = 75 °C, 80 °C, 85 °C and 90 °C) was monitored over time (see Fig. S25–S28, ESI†). An inversion barrier characterised by $\Delta H_e^{\ddagger} = 39 \pm 1$ (kcal mol^{-1}) and $\Delta S_e^{\ddagger} = 26 \pm 1$ (cal K^{-1} mol^{-1}) was found (see Table S10, ESI†). This results in a Gibbs free energy of activation for the enantiomerisation process ($\Delta G_e^{\ddagger}$) of 31 ± 2 (kcal mol^{-1}) at 298 K. (**P**)-**Hel-DiDiKTa** possesses a similar inversion barrier (298 K) to other double helicenes found in the literature (Table S10, ESI†).[105,106] (**P**)-**Hel-DiDiKTa** also appears to have a similar enantiomerisation barrier to other bridged phenylamines previously reported (Table S10, ESI†).[107,108] Moreover, when compared to [5] and [6]-helicene (f and g in Table S10, ESI†), (**P**)-**Hel-DiDiKTa** possesses a similar barrier as [6]helicene.[109] The half-life obtained for the enantiomerisation is *ca.* 310 years at room temperature.

Not only is (**P**)-**Hel-DiDiKTa** stable to enantiomerization but the compound is also stable towards thermal decomposition. Thermogravimetric analysis (TGA) showed that no decomposition was observed in the temperature range of the enantiomerization study and the decomposition temperature was found to be 399 °C, corresponding to 5% weight loss (Fig. S30, ESI†).

In summary, we report a novel S-shaped triphenylamine diketone double [4]helicene that exhibits MR-TADF. Unlike the previously reported triphenylamine diketone helicene (**Hel-DiKTa-2**), **Hel-DiDiKTa** was predicted by SCS-CC2 calculations to show a ΔE_{ST} appropriate for TADF, which was confirmed experimentally (0.15 eV in 1 wt% doped mCP film). As expected from a MR-TADF emitter, the emission peak at 473 nm is narrow, with a FWHM of 44 nm in toluene, a value considerably smaller than often observed for helicenoids. In 1 wt% mCP the emission peak at 477 nm shows a FWHM value of 50 nm. The TADF behavior of **Hel-DiDiKTa** was confirmed by temperature-dependent time-resolved photoluminescence measurements, and the chiroptical behavior of the enantiomers was determined, with a maximum $|g_{abs}|$ of 2.8×10^{-3} and a $|g_{PL}|$ of 4×10^{-4}. While the low Φ_{PL} precluded the use of this compound as an emitter in OLEDs, we believe that this report will serve as a foundation to develop intrinsically chiral, CPL-active MR-TADF molecules for OLEDs. Further work is undergoing in our lab to improve the optoelectronic and chiroptical properties of chiral MR-TADF compounds. Finally, the enantiomerization studies and the thermogravimetric analysis demonstrate the high inherent stability of (**P**)-**Hel-DiDiKTa**.

Conflicts of interest

The authors declare that they have no conflict of interest.

Acknowledgements

This journal is © The Royal Society of Chemistry 2022

J. Mater. Chem. C, 2022, **10**, 4861–4870 | **4867**

References

1 F. Saal, F. Zhang, M. Holzapfel, M. Stolte, E. Michail, M. Moos, A. Schmiedel, A. M. Krause, C. Lambert, F. Würthner and P. Ravat, *J. Am. Chem. Soc.*, 2020, **142**, 21298–21303.

2 K. Dhbaibi, L. Favereau and J. Crassous, *Chem. Rev.*, 2019, **119**, 8846–8953.

3 Y. Nakai, T. Mori and Y. Inoue, *J. Phys. Chem. A*, 2012, **112**, 7372–7385.

4 Y. Shen and C. Chen, *Chem. Rev.*, 2012, **112**, 1463–1535.

5 K. Dhbaibi, L. Abella, S. Meunier-Della-Gatta, T. Roisnel, N. Vanthuyne, B. Jamoussi, G. Pieters, B. Racine, E. Quesnel, J. Autschbach, J. Crassous and L. Favereau, *Chem. Sci.*, 2021, **12**, 5522–5533.

6 C. Shen, G. Zhang, Y. Ding, N. Yang, F. Gan, J. Crassous and H. Qiu, *Nat. Commun.*, 2021, **12**, 2786.

7 H. Tanaka, Y. Inoue and T. Mori, *ChemPhotoChem*, 2018, **2**, 386–402.

8 J. L. Greenfield, J. Wade, J. R. Brandt, X. Shi, T. J. Penfold and J. Fuchter, *Chem. Sci.*, 2021, **12**, 1–15.

9 W. L. Zhao, M. Li, H. Y. Lu and C. F. Chen, *Chem. Commun.*, 2019, **55**, 13793–13803.

10 T. Verbiest, S. Van Elshocht, M. Kauranen, L. Hellemans, J. Snauwaert, C. Nuckolls, T. J. Katz and A. Persoons, *Science*, 1998, **282**, 913–916.

11 O. Kel, A. Fürstenberg, N. Mehanna, C. Nicolas, B. Laleu, M. Hammarson, B. Albinsson, J. Lacour and E. Vauthey, *Chem. – A Eur. J.*, 2013, **19**, 7173–7180.

12 S. D. Dreher, T. J. Katz, K. Lam and A. L. Rheingold, *J. Org. Chem.*, 2000, **65**, 815–822.

13 K. Yavari, P. Aillard, Y. Zhang, F. Nuter, P. Retailleau, A. Voituriez and A. Marinetti, *Angew. Chem., Int. Ed.*, 2014, **53**, 861–865.

14 J. E. Field, G. Muller, J. P. Riehl and D. Venkataraman, *J. Am. Chem. Soc.*, 2003, **125**, 11808–11809.

15 H. Kubo, D. Shimizu, T. Hirose and K. Matsuda, *Org. Lett.*, 2020, **22**, 9276–9281.

16 H. Kubo, T. Hirose, T. Nakashima, T. Kawai, J. Hasegawa and K. Matsuda, *J. Phys. Chem. Lett.*, 2021, **12**, 686–695.

17 J. Han, S. Guo, H. Lu, S. Liu, Q. Zhao and W. Huang, *Adv. Opt. Mater.*, 2018, **6**, 1800538.

18 D. Zhang, M. Li and C. Chen, *Chem. Soc. Rev.*, 2020, **49**, 1331–1343.

19 S. Sahasithiwat, T. Mophuang, L. Menbangpung, S. Kamtonwong and T. Sooksimuang, *Synth. Met.*, 2010, **160**, 1148–1152.

20 L. Wan, X. Shi, J. Wade, A. J. Campbell and M. J. Fuchter, *Adv. Opt. Mater.*, 2021, **9**, 2100066.

21 L. Wan, J. Wade, F. Salerno, O. Arteaga, B. Laidlaw, X. Wang, T. Penfold, M. J. Fuchter and A. J. Campbell, *ACS Nano*, 2019, **13**, 8099–8105.

22 J. Wade, J. N. Hilfiker, J. R. Brandt, L. Liirò-Peluso, L. Wan, X. Shi, F. Salerno, S. T. J. Ryan, S. Schöche, O. Arteaga, T. Jávorfi, G. Siligardi, C. Wang, D. B. Amabilino, P. H. Beton, A. J. Campbell and M. J. Fuchter, *Nat. Commun.*, 2020, **11**, 1–11.

23 Y. Yang, R. C. Da Costa, D. M. Smilgies, A. J. Campbell and M. J. Fuchter, *Adv. Mater.*, 2013, **25**, 2624–2628.

24 A. Klimash, P. Pander, W. T. Klooster, S. J. Coles, P. Data, F. B. Dias and P. J. Skabara, *J. Mater. Chem. C*, 2018, **6**, 10557–10568.

25 M. Li, Y. Wang, D. Zhang, D. Zhang, Z. Hu, L. Duan and C. Chen, *Sci. China Mater.*, 2021, **64**, 899–908.

26 Y. Wei, A. Zheng, X. Xie, J. Zhang, L. He and P. Wang, *ACS Mater. Lett.*, 2021, **3**, 947–955.

27 Y. S. Lin, S. Y. Abate, C. I. Wang, Y. S. Wen, C. I. Chen, C. P. Hsu, C. C. Chueh, Y. T. Tao and S. S. Sun, *ACS Appl. Mater. Interfaces*, 2021, **13**, 20051–20059.

28 J. Wang, Y. Wang, X. Xie, Y. Ren, B. Zhang, L. He, J. Zhang, L. D. Wang and P. Wang, *ACS Energy Lett.*, 2021, **6**, 1764–1772.

29 N. R. Paisley, C. M. Tonge and Z. M. Hudson, *Front. Chem.*, 2020, **8**, 229.

30 C. Adachi and A. S. D. Sandanayaka, *CCS Chem.*, 2020, **2**, 1203–1216.

31 X. Wang, D. Zhou, J. Huang and J. Yu, *Appl. Phys. Lett.*, 2015, **107**, 043303.

32 M. A. Bryden and E. Zysman-Colman, *Chem. Soc. Rev.*, 2021, **50**, 7587–7680.

33 V. N. Nguyen, A. Kumar, M. H. Lee and J. Yoon, *Coord. Chem. Rev.*, 2020, **425**, 213545.

34 M. Y. Wong and E. Zysman-Colman, *Adv. Mater.*, 2017, **29**, 1–54.

35 H. Uoyama, K. Goushi, K. Shizu, H. Nomura and C. Adachi, *Nature*, 2012, **492**, 234–238.

36 G. Méhes, H. Nomura, Q. Zhang, T. Nakagawa and C. Adachi, *Angew. Chem., Int. Ed.*, 2012, **51**, 11311–11315.

37 T. Nakagawa, S. Y. Ku, K. T. Wong and C. Adachi, *Chem. Commun.*, 2012, **48**, 9580–9582.

38 S. Hirata, Y. Sakai, K. Masui, H. Tanaka, S. Y. Lee, H. Nomura, N. Nakamura, M. Yasumatsu, H. Nakanotani, Q. Zhang, K. Shizu, H. Miyazaki and C. Adachi, *Nat. Mater.*, 2015, **14**, 330–336.

39 C. A. Parker and C. G. Hatchard, *Trans. Faraday Soc.*, 1961, **57**, 1894–1904.

40 H. W. Chen, J. H. Lee, B. Y. Lin, S. Chen and S. T. Wu, *Light: Sci. Appl.*, 2018, **7**, 17168.

4868 | *J. Mater. Chem. C*, 2022, **10**, 4861–4870

This journal is © The Royal Society of Chemistry 2022

41 T. Hatakeyama, K. Shiren, K. Nakajima, S. Nomura, S. Nakatsuka, K. Kinoshita, J. Ni, Y. Ono and T. Ikuta, *Adv. Mater.*, 2016, **28**, 2777–2781.

42 Y. Kondo, K. Yoshiura, S. Kitera, H. Nishi, S. Oda, H. Gotoh, Y. Sasada, M. Yanai and T. Hatakeyama, *Nat. Photonics*, 2019, **13**, 678–682.

43 Y. Zhang, D. Zhang, T. Huang, A. J. Gillett, Y. Liu, D. Hu, L. Cui, Z. Bin, G. Li, J. Wei and L. Duan, *Angew. Chem., Int. Ed.*, 2021, **60**, 20498–20503.

44 D. Hall, S. M. Suresh, P. L. dos Santos, E. Duda, S. Bagnich, A. Pershin, P. Rajamalli, D. B. Cordes, A. M. Z. Slawin, D. Beljonne, A. Köhler, I. D. W. Samuel, Y. Olivier and E. Zysman-Colman, *Adv. Opt. Mater.*, 2020, **8**, 1901627.

45 H. Min, I. S. Park and T. Yasuda, *Angew. Chem., Int. Ed.*, 2021, **60**, 7643–7648.

46 F. Chen, L. Zhao, X. Wang, Q. Yang, W. Li, H. Tian, S. Shao, L. Wang, X. Jing and F. Wang, *Sci. China: Chem.*, 2021, **64**, 547–551.

47 J. Wei, C. Zhang, D. Zhang, Y. Zhang, Z. Liu, Z. Li, G. Yu and L. Duan, *Angew. Chem., Int. Ed.*, 2021, **60**, 12269–12273.

48 S. Oda, W. Kumano, T. Hama, R. Kawasumi, K. Yoshiura and T. Hatakeyama, *Angew. Chem., Int. Ed.*, 2021, **60**, 2882–2886.

49 D. Sun, S. M. Suresh, D. Hall, M. Zhang, C. Si, D. B. Cordes, A. M. Z. Slawin, Y. Olivier, X. Zhang and E. Zysman-Colman, *Mater. Chem. Front.*, 2020, **4**, 2018–2022.

50 N. Ikeda, S. Oda, R. Matsumoto, M. Yoshioka, D. Fukushima, K. Yoshiura, N. Yasuda and T. Hatakeyama, *Adv. Mater.*, 2020, **32**, 2004072.

51 S. Zou, C. Peng, S. Yang, Y. Qu, Y. Yu, X. Chen, Z. Jiang and L. Liao, *Org. Lett.*, 2021, **23**, 958–962.

52 Y. Qi, W. Ning, Y. Zou, X. Cao, S. Gong and C. Yang, *Adv. Funct. Mater.*, 2021, **2102017**, 1–7.

53 M. Yang, I. S. Park and T. Yasuda, *J. Am. Chem. Soc.*, 2020, **142**, 19468–19472.

54 F. Huang, K. Wang, Y. Z. Shi, X. C. Fan, X. Zhang, J. Yu, C. S. Lee and X. H. Zhang, *ACS Appl. Mater. Interfaces*, 2021, **13**, 36089–36097.

55 S. Madayanad Suresh, D. Hall, D. Beljonne, Y. Olivier and E. Zysman-Colman, *Adv. Funct. Mater.*, 2020, **30**, 1908677.

56 Y. Zhang, J. Wei, D. Zhang, C. Yin, G. Li, Z. Liu, X. Jia, J. Qiao and L. Duan, *Angew. Chem., Int. Ed.*, 2022, **61**, e202113206.

57 P. Jiang, J. Miao, X. Cao, H. Xia, K. Pan, T. Hua, X. Lv, Z. Huang, Y. Zou and C. Yang, *Adv. Mater.*, 2021, 2106954.

58 T. Imagawa, S. Hirata, K. Totani, T. Watanabe and M. Vacha, *Chem. Commun.*, 2015, **51**, 13268–13271.

59 M. Li, S. Li, D. Zhang, M. Cai, L. Duan, M. Fung and C. Chen, *Angew. Chem., Int. Ed.*, 2018, **57**, 2889–2893.

60 L. Zhou, G. Xie, F. Ni and C. Yang, *Appl. Phys. Lett.*, 2020, **117**, 130502.

61 J. R. Brandt, F. Salerno and M. J. Fuchter, *Nat. Rev. Chem.*, 2017, **1**, 0045.

62 X. Li, Y. Xie and Z. Li, *Adv. Photonics Res.*, 2021, **2**, 2000136.

63 T. Y. Li, Y. M. Jing, X. Liu, Y. Zhao, L. Shi, Z. Tang, Y. X. Zheng and J. L. Zuo, *Sci. Rep.*, 2015, **5**, 14912.

64 J. F. Sherson, H. Krauter, R. K. Olsson, B. Julsgaard, K. Hammerer, I. Cirac and E. S. Polzik, *Nature*, 2006, **443**, 557–560.

65 Y. Deng, M. Wang, Y. Zhuang, S. Liu, W. Huang and Q. Zhao, *Light Sci. Appl.*, 2021, **10**, 1–18.

66 R. Farshchi, M. Ramsteiner, J. Herfort, A. Tahraoui and H. T. Grahn, *Appl. Phys. Lett.*, 2011, **98**, 162508.

67 Y. Yang, R. Correa, M. J. Fuchter and A. J. Campbell, *Nat. Photonics*, 2013, **7**, 634–638.

68 J. Jiménez, L. Cerdán, F. Moreno, B. L. Maroto, I. García-Moreno, J. L. Lunkley, G. Muller and S. De La Moya, *J. Phys. Chem. C*, 2017, **121**, 5287–5292.

69 R. Tempelaar, A. Stradomska, J. Knoester and F. C. Spano, *J. Phys. Chem. B*, 2011, **115**, 10592–10603.

70 T. Wu, P. Bouř and V. Andrushchenko, *Sci. Rep.*, 2019, **9**, 1068.

71 P. M. L. Blok and H. P. J. M. Dekkers, *Chem. Phys. Lett.*, 1989, **161**, 188–194.

72 J. A. Schellman, *Chem. Rev.*, 1975, **75**, 323–331.

73 R. Carr, N. H. Evans and D. Parker, *Chem. Soc. Rev.*, 2012, **41**, 7673–7686.

74 F. Zinna and L. D. I. Bari, *Chirality*, 2015, **27**, 1–13.

75 J. L. Lunkley, D. Shirotani, K. Yamanari, S. Kaizaki and G. Muller, *J. Am. Chem. Soc.*, 2008, **130**, 13814–13815.

76 L. Arrico, L. Di Bari and F. Zinna, *Chem. – A Eur. J.*, 2021, **27**, 2920–2934.

77 E. M. Sánchez-Carnerero, A. R. Agarrabeitia, F. Moreno, B. L. Maroto, G. Muller, M. J. Ortiz and S. De La Moya, *Chem. – A Eur. J.*, 2015, **21**, 13488–13500.

78 N. Chen and B. Yan, *Molecules*, 2018, **23**, 3376.

79 Z. L. Tu, Z. P. Yan, X. Liang, L. Chen, Z. G. Wu, Y. Wang, Y. X. Zheng, J. L. Zuo and Y. Pan, *Adv. Sci.*, 2020, **7**, 1–6.

80 Z. Wu, H. Han, Z. Yan, X. Luo, Y. Wang and Y. Zheng, *Adv. Mater.*, 2019, **31**, 1900524.

81 Y. Li, A. Yagi and K. Itami, *J. Am. Chem. Soc.*, 2020, **142**, 3246–3253.

82 L. Frédéric, A. Desmarchelier, R. Plais, L. Lavnevich, G. Muller, C. Villafuerte, G. Clavier, E. Quesnel, B. Racine, S. Meunier-della-gatta, J. Dognon, P. Thuéry, J. Crassous, L. Favereau and G. Pieters, *Adv. Funct. Mater. Mater.*, 2020, **30**, 2004838.

83 Y.-P. Zhang, X. Liang, X.-F. Luo, S.-Q. Song, S. Li, Y. Wang, Z.-P. Mao, W.-Y. Xu, Y.-X. Zheng, J.-L. Zuo and Y. Pan, *Angew. Chem., Int. Ed.*, 2021, **60**, 8435–8440.

84 Y. Xu, Q. Wang, X. Cai, C. Li and Y. Wang, *Adv. Mater.*, 2021, 2100652.

85 S.-Y. Yang, S.-N. Zou, F.-C. Kong, X.-J. Liao, Y.-K. Qu, Z.-Q. Feng, Y.-X. Zheng, Z.-Q. Jiang and L.-S. Liao, *Chem. Commun.*, 2021, **57**, 11041–11044.

86 X. Wu, J. Huang, B. Su, S. Wang, L. Yuan, W. Zheng, H. Zhang, Y. Zheng, W. Zhu and P. Chou, *Adv. Mater.*, 2021, 2105080.

87 J.-K. Li, X.-Y. Chen, Y.-L. Guo, X.-C. Wang, A. C.-H. Sue, X.-Y. Cao and X.-Y. Wang, *J. Am. Chem. Soc.*, 2021, **143**, 17958–17963.

88 J. E. Field, T. J. Hill and D. Venkataraman, *J. Org. Chem.*, 2003, **68**, 6071–6078.

This journal is © The Royal Society of Chemistry 2022

J. Mater. Chem. C, 2022, **10**, 4861–4870 | **4869**

89 T. Mori, *Chem. Rev.*, 2021, **121**, 2373–2412.

90 N. J. Schuster, L. A. Joyce, D. W. Paley, F. Ng, M. L. Steigerwald and C. Nuckolls, *J. Am. Chem. Soc.*, 2020, **142**, 7066–7074.

91 Q. Jiang, Y. Han, Y. Zou, H. Phan, L. Yuan, T. Herng, J. Ding and C. Chi, *Chem. – A Eur. J.*, 2020, **26**, 5613–15622.

92 S. Kinoshita, R. Yamano, Y. Shibata, Y. Tanaka, K. Hanada, T. Matsumoto, K. Miyamoto, A. Muranaka, M. Uchiyama and K. Tanaka, *Angew. Chem., Int. Ed.*, 2020, **59**, 11020–11027.

93 G. Zhang, J. Tan, L. Zhou, C. Liu, J. Liu, Y. Zou, A. Narita and Y. Hu, *Org. Lett.*, 2021, **23**, 6183–6188.

94 N. G. Connelly and W. E. Geiger, *Chem. Rev.*, 1996, **96**, 877–910.

95 H. Tanaka, M. Ikenosako, Y. Kato, M. Fujiki, Y. Inoue and T. Mori, *Commun. Chem.*, 2018, **1**, 38.

96 A. Pershin, D. Hall, V. Lemaur, J. C. Sancho-Garcia, L. Muccioli, E. Zysman-Colman, D. Beljonne and Y. Olivier, *Nat. Commun.*, 2019, **10**, 597.

97 X. Wu, B. K. Su, D. G. Chen, D. Liu, C. C. Wu, Z. X. Huang, T. C. Lin, C. H. Wu, M. Zhu, E. Y. Li, W. Y. Hung, W. Zhu and P. T. Chou, *Nat. Photonics*, 2021, **15**, 780–786.

98 J. A. Knçller, G. Meng, X. Wang, D. Hall, A. Pershin, D. Beljonne, Y. Olivier, S. Laschat, E. Zysman-colman and S. Wang, *Angew. Chem., Int. Ed.*, 2020, **59**, 3156–3160.

99 S. M. Suresh, E. Duda, D. Hall, Z. Yao, S. Bagnich, D. Beljonne, M. Buck, Y. Olivier, A. Ko, A. M. Z. Slawin, H. Ba and E. Zysman-colman, *J. Am. Chem. Soc.*, 2020, **142**, 6588–6599.

100 M. K. Etherington, J. Gibson, H. F. Higginbotham, T. J. Penfold and A. P. Monkman, *Nat. Commun.*, 2016, **7**, 13680.

101 Y. Wada, H. Nakagawa, S. Matsumoto, Y. Wakisaka and H. Kaji, *Nat. Photonics*, 2020, **14**, 643–649.

102 C. Y. Chan, M. Tanaka, Y. T. Lee, Y. W. Wong, H. Nakanotani, T. Hatakeyama and C. Adachi, *Nat. Photonics*, 2021, **15**, 203–207.

103 J. U. Kim, I. S. Park, C. Y. Chan, M. Tanaka, Y. Tsuchiya, H. Nakanotani and C. Adachi, *Nat. Commun.*, 2020, **11**, 1–8.

104 Y. Y. Pan, J. Huang, Z. M. Wang, D. W. Yu, B. Yang and Y. G. Ma, *RSC Adv.*, 2017, **7**, 26697–26703.

105 Q. Jiang, Y. Han, Y. Zou, H. Phan, L. Yuan, T. S. Herng, J. Ding and C. Chi, *Chem. – A Eur. J.*, 2020, **26**, 15613–15622.

106 T. Katayama, S. Nakatsuka, H. Hirai, N. Yasuda, J. Kumar, T. Kawai and T. Hatakeyama, *J. Am. Chem. Soc.*, 2016, **138**, 5210–5213.

107 B. D. Gliemann, A. G. Petrovic, E. M. Zolnhofer, P. O. Dral, F. Hampel, G. Breitenbruch, P. Schulze, V. Raghavan, K. Meyer, P. L. Polavarapu, N. Berova and M. Kivala, *Chem. – Asian J.*, 2017, **12**, 31–35.

108 H. Nishimura, K. Tanaka, Y. Morisaki, Y. Chujo, A. Wakamiya and Y. Murata, *J. Org. Chem.*, 2017, **82**, 5242–5249.

109 R. H. Martin and M. J. Marchant, *Tetrahedron Lett.*, 1972, **13**, 3707–3708.

4870 | *J. Mater. Chem. C*, 2022, **10**, 4861–4870

This journal is © The Royal Society of Chemistry 2022